ACS APPLIED MATERIALS & INTERFACES

Research Article

www.acsami.org

Effect of Octacalcium-Phosphate-Modified Micro/Nanostructured Titania Surfaces on Osteoblast Response

Pinliang Jiang,[†,‡] Jianhe Liang,[‡] Ran Song,[‡] Yanmei Zhang,[‡] Lei Ren,[†,‡] Lihai Zhang,[§] Peifu Tang,*[,§] and Changjian Lin*[,†,‡]

[†]College of Materials and [‡]State Key Lab of Physical Chemistry of Solid Surfaces, Department of Chemistry, College of Chemistry and Chemical Engineering, Xiamen University, Xiamen 361005, China

[§]Department of Orthopaedics, General Hospital of Chinese PLA, Beijing 100853, China

ABSTRACT: Surface structures and properties of titanium implants play a vital role in successful bone replacement. To mimic the natural bone structure, some strategies have recently focused on the preparation of multiscaled morphology on medical titanium and shown some promising results; however, relatively few efforts have been made for further enhancing the biocompatibility of such a hierarchical hybrid structure without compromising the superior bioactivity of the starting micro/nano roughness. In this study, a thin ribbonlike octacalcium phosphate (OCP) coating was electrodeposited on a hierarchically structured titania surface, maintaining its micro/nanospongelike morphology. It is indicated that the micro/nanostructured surface with deposited OCP showed an improved biomineralization ability, in comparison to that without OCP modification, when immersed in simulated body fluid (SBF). Further evaluations of cellular activities demonstrated that the introduction of OCP to the micro/nano spongelike-structured surface remarkably enhanced MC3T3-E1 cell proliferation, alkaline phosphatase activity, and extracellular matrix mineralization compared to that of cells on the micro/nanospongelike titania surface during 14 days of culturing. Meanwhile, the OCP-deposited micro/nanostructured surface displayed much a smaller passive current density and lower current response to the applied potential, resulting in the improvement of corrosion resistance. All of the evaluations suggested that the modification of the OCP coating on the prepared micro/nanospongelike titania is of superior chemical stability, biomineralization, and osteoblast activities, which indicates a favorable implant microenvironment for osseointegration in vivo.

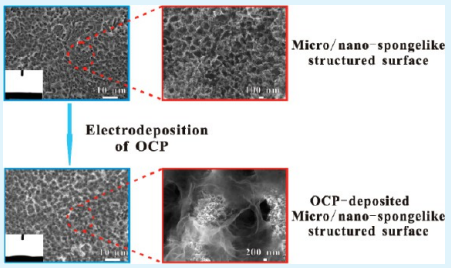

KEYWORDS: *titania, octacalcium phosphate, corrosion resistance, apatite, cellular activities*

1. INTRODUCTION

Hard tissues often suffer from injuries because of aging, accidents, and other causes. In certain cases, it is common to substitute the injured hard tissues with artificial materials. Titanium and its alloys have been vastly used for hard tissue replacements such as dental and orthopedic implants due to their moderate elastic modulus, excellent corrosion resistance, and favorable biocompatibility.[1] However, the native oxide layer on titanium metals is bioinert, and it is generally encapsulated by a fibrous tissue layer without producing osseointegration with the surrounding tissue after implantation. Previous studies have indicated that the surface characteristics of implants play a critical role in determining the cell and tissue responses.[1,2] Surface characteristics such as surface topography, wettability, roughness, and composition have been reported to markedly modulate protein adsorption and cell proliferation and differentiation in vitro and influence bone-to-implant contact as well as bone regeneration in vivo.[3,4] Hence, to achieve a desirable integration ability of titanium implants with bones, various surface modifications have been adopted to enable the substrates with specific properties to improve the bioactivity, including plasma immersion ion implantation,[5] deposition of calcium phosphate coatings,[6] and immobilization of biomolecules.[7,8] Among them, calcium phosphate compounds attract great attention because CaP ceramics are considered to be a class of bioactive materials, and they possess much better chemical stability during preparation and storage in comparison to that of biomolecules.

It is reported that octacalcium phosphate (OCP) appears to be osteoconductive and is able to endow materials with favorable bioactivity.[9] Dekker et al. observed that the crystalline OCP-coated Ti6Al4V discs presented a superior volume of newly generated bone formation after implantation in mice.[10] Kikawa et al. suggested that OCP was a proposed precursor of bone apatite crystals and involved in intramembranous bone formation when implanted in mouse calvaria.[11] Although the exact mechanism is still unclear, the stimulatory capability of OCP to enhance osteoconductivity is generally ascribed to the physicochemical change caused by the process of converting OCP to hydroxyapatite (HA), accompanying the consumption and release of Ca^{2+} and PO_4^{3-}.[12] In some cases, OCP was observed to be more capable than several HA coatings (Ca-deficient HA obtained via precipitation and sintered or nonsintered HA with a Ca/P molar ratio of 1.67) of promoting

Received: April 13, 2015
Accepted: June 15, 2015
Published: June 15, 2015

DOI: 10.1021/acsami.5b03172
ACS Appl. Mater. Interfaces 2015, 7, 14384−14396

bone formation when implanted in bone defects.[12] Thus, the use of OCP as a source material for bioactive bone substitutes has driven many promising efforts.

Natural bone is a hierarchical porous structure assembled from macrostructure to nanostructure.[13] To develop a biomimic structure, some recent studies have examined the effects of a hierarchical structure, composed of both micro- and nanoscale building blocks, on cellular responses.[14−16] For instance, nanoscale features such as TiO_2 nanotubes,[14] nanonodules,[15] and nanoprotuberances[16] have been added to microroughened titanium surfaces, and such works have indicated that a micro/nano hybrid structure on surfaces was able to markedly enhance cell adhesion, morphology, proliferation, and differentiation. However, in some cases, either a decreased proliferation[17] or a reduced gene expression of osteopontin (OPN) and osteocalcin (OCN)[18] was also detected on the micro/nanostructure. Accordingly, although some promising results have been reported, optimizing the surface composition and property for the improvement of the bioactivity of titanium implants is still needed. To our knowledge, the investigation of the further modification of such micro/nano hybrid structured surfaces without greatly changing other underlying characteristics (e.g., surface morphology and surface wettability) is rarely reported yet.

In this study, a combined mode was adopted to prepare a tailored hierarchical micro/nanostructured surface on Ti substrates. The OCP-induced surface modification process of micro/nanospongelike TiO_2 film on Ti substrates was formed by a combined acid-etching and anodization treatment and then followed by the electrodeposition of a thin OCP layer on the prepared micro/nanospongelike-structured surfaces without greatly altering the original micro/nano feature, wettability, and other surface characteristics, but with the expectations of regulating and stimulating cell adhesion, growth, and differentiation. The surface composition and wettability were confirmed by various physicochemical methods. Meanwhile, the cell responses, including proliferation and differentiation as well as extracellular matrix mineralization to the constructed surfaces, were systematically characterized to evaluate the effects of the OCP-induced hierarchical hybrid structures on the biological functions of osteoblasts in vitro.

2. EXPERIMENTAL DETAILS

2.1. Preparation of Surfaces. Commercial pure titanium discs (15 mm in diameter and 2 mm in thickness) were polished by grit SiC papers from no. 400 to no.1000 and then ultrasonically cleaned in acetone, alcohol, and distilled water for 10 min, respectively (designated as PTi). To obtain a micro/nanospongelike structure on the titanium surfaces, we etched the substrates in a mixed-acid solution containing 48% H_2SO_4 and 18% HCl for 1 h at 75 °C, performed anodization in an ethylene glycol solution composed of 0.3 wt % NH_4F and 0.2 wt % H_2O_2 at 50 V for 30 min, and then annealed the substrates at 450 °C for 2 h (designated as MS-450).

The electrodeposition of OCP on micro/nanospongelike-structured surfaces was conducted in a two-electrode cell with the above MS-450 disc as a working electrode and a platinum plate as a counter electrode. The electrolyte was composed of 0.042 M $Ca(NO_3)_2$ and 0.025 M $NH_4H_2PO_4$, and its pH was adjusted to 4.20 by 0.1 M NaOH.[19] The electrodeposition process lasted for 1 min with a current density of 0.5 mA/cm^2 (designated as MS-450−OCP). For comparison, the polished titanium was subjected to electrodeposition in the above electrolyte as well (designated as PTi−OCP).

2.2. Surface Characterization. The surface morphology of the samples was evaluated using a field emission scanning electron microscope (FESEM; Hitachi S4800, Japan). Phase identification of the samples was measured using an X-ray diffractometer (XRD; PANalytical X′pert PRO, Holland) with a Cu−Kα radiation source at 40 kV and 30 mA.

2.3. Contact Angle Measurement. The contact angles of different titanium samples were obtained by using a contact angle goniometer (Kruss DSA100, Germany) equipped with a digital camera and image analysis software. A 5 μL water droplet was dropped onto each substrate, and then the image was captured and analyzed with the software to obtain the contact angle of the air−liquid substrate interface. Prior to measurement, the substrates were carefully cleaned by distilled water and dried in a desiccator overnight. A total of three samples were measured for each group.

2.4. Corrosion Resistance Test. The potentiodynamic polarization and chrono-amperometric measurements were measured in a three-electrode electrochemical cell in PBS solution (8.0 g/L NaCl, 0.2 g/L KCl, 3.58 g/L $Na_2HPO_4{\cdot}12H_2O$, and 0.24 g/L KH_2PO_4 with a pH of approximately 7.40) at 37 °C by using an Autolab PGSTAT 30 electrochemical workstation. All of the Ti samples with an exposed area (1 cm × 1 cm) were prepared as working electrodes, a platinum plate as the counter electrode, and a saturated calomel electrode (SCE) as the reference electrode. The potentiodynamic polarization curves were measured by scanning from −0.5 to +1.0 V from the respective open circuit potential at a rate of 0.5 mV/s. Chrono-amperometric measurements were carried out at an applied potential of 0.5 V (versus SCE) for 30 min to record the current response to this applied potential. The applied potential of 0.5 V (versus SCE) was close to body potential.[20]

2.5. Simulated Body Fluid Immersion Test. The various samples were immersed in simulated body fluid (SBF) to evaluate the in vitro apatite precipitation. The SBF solution was obtained based on Kokubo's formulation by dissolving 8.035 g/L NaCl, 0.355 g/L $NaHCO_3$, 0.225 g/L KCl, 0.231 g/L $K_2HPO_4{\cdot}3H_2O$, 0.311 g/L $MgCl_2{\cdot}6H_2O$, 0.292 g/L $CaCl_2$, and 0.072 g/L Na_2SO_4 in distilled water and then buffered at pH 7.40 with Tris and 1 M HCl.[21] After being immersed in SBF solution for 6 days, the samples were taken out of the solution, rinsed with distilled water, and air-dried.

2.6. Protein Adsorption Assay. A droplet of 1 mL α-MEM containing 10% fetal bovine serum (FBS) was pipetted onto each sample. After incubating for 2 h at 37 °C, the samples were transferred to a new 24-well plate and washed with PBS. A total of 500 μL of 1% sodium dodecyl sulfate (SDS) solution was then added to each well to detach the adsorbed protein. The protein content in the SDS solution was determined using a BCA protein assay kit (Applygen Technologies Inc., China).

2.7. In Vitro Cell Culture. Mouse MC3T3-E1 preosteoblastic cells were used in the biological assays. The cells were cultured in α-MEM supplemented with 10% FBS, 100 units/mL penicillin, and 100 μg/mL streptomycin and maintained under a humidified atmosphere with 5% CO_2 at 37 °C. After reaching 90% of confluence, the cells were detached from the culture dish with 0.25% trypsin, centrifuged at 1000 rpm for 5 min, and resuspended in fresh culture medium for subsequent assays. All of the samples were sterilized by 75% alcohol for 1 h and then placed into a 24-well plate and seeded with cells at a density of 2 × 10^4 cells/mL. The culture medium was replaced every 2 days.

2.8. Lactate Dehydrogenase Activity Assay. The lactate dehydrogenase activity (LDH) was assayed as an index of the cytotoxicity of the samples. After 24 h of incubation, the culture medium was collected and centrifuged at 500 g, and the supernatant was measured according to the LDH kit instructions (Nanjing Jiancheng Bioengineering Institute, China).

2.9. Cell Adhesion. MC3T3-E1 cells were seeded on the substrates at a density of 2 × 10^4 cells/well. After incubating for 30, 60, and 120 min, the samples were rinsed with PBS to remove the nonadherent cells. Cells were fixed with 4% paraformaldehyde for 2 h and stained by 4′-6′-diamidino-2-phenylindole (DAPI). The cells were then photographed under a fluorescence microscope (Nikon Ti−U, Japan) and analyzed using ImageJ software.

2.10. Cell Morphology. After 1 and 14 days of incubation, the cells on the samples were gently rinsed with phosphate buffer saline

DOI: 10.1021/acsami.5b03172
ACS Appl. Mater. Interfaces 2015, 7, 14384−14396

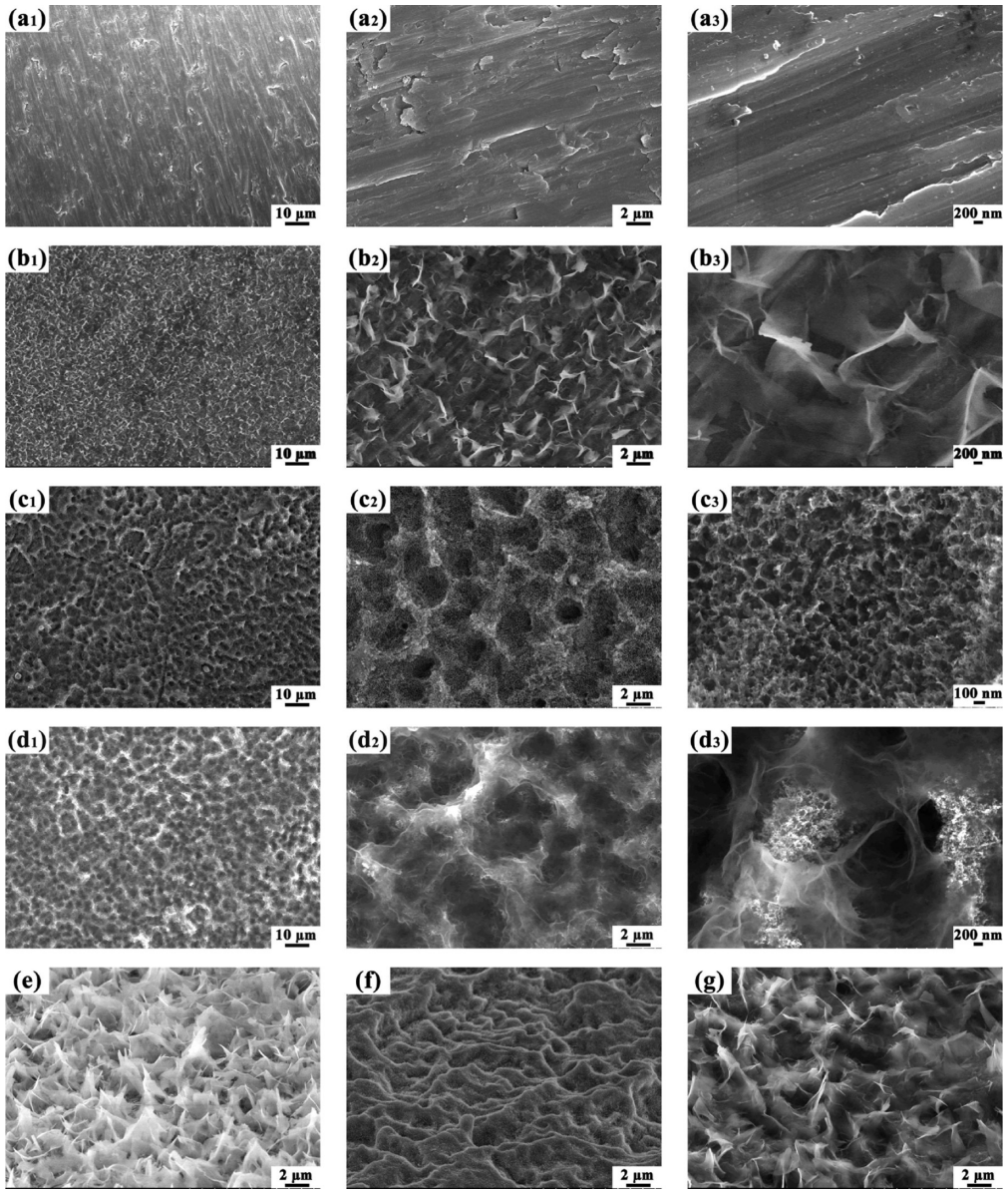

Figure 1. SEM micrographs of the prepared samples: (a) PTi, (b) PTi−OCP, (c) MS-450, and (d) MS-450−OCP. Parts e−g are the titled micrographs of (b) PTi−OCP, (c) MS-450, and (d) MS-450−OCP, respectively. Parts a_2−d_2 are high-magnification images of the samples in a_1−d_1, respectively, and parts a_3−d_3 are high-magnification images of the samples in parts a_2−d_2, respectively.

(PBS), fixed with 2.5% glutaraldehyde, and dehydrated in graded concentrations of ethanol (30, 50, 70, 90, and 100%). Afterward, the samples were dried in a freeze-dryer (Eyela FDU-1200, Tokyo Rikakikai, Japan), sputtered with a thin platinum layer, and observed by SEM.

2.11. Cell Proliferation. An MTT assay was used to evaluate the cell proliferation. After 1, 4, and 7 days of cell culturing, 200 μL of MTT solution (5 mg/mL) was added to each well and incubated for another 4 h at 37 °C to form formazan crystals. The MTT-containing medium was then discarded, and 1 mL of dimethyl sulfoxide was added to dissolve the formazan. The optical density (OD) at 490 nm was measured using a multimode microplate reader (Tecan Infinite M200, Switzerland).

2.12. Alkaline Phosphatase Activity Assay. The early retention of the osteoblastic phenotype was evaluated by measuring the alkaline phosphatase (ALP) activity with an ALP kit (Jiancheng Bioengineering Institute, China). After incubating for 7 and 14 days, the incubated cells on the samples were washed thrice with PBS, and 500 ul of 0.2% Triton X-100 was added to each well to extract the intracellular phospatase. The absorbance of ALP activity at 520 nm was measured with a microplate reader, and the ALP activity was normalized to the total protein content.

2.13. Collagen Secretion Assay. The collagen secretion was determined and quantified by Sirius Red staining. After incubating for 7 and 14 days, cells on the samples were washed with PBS and fixed with 4% paraformaldehyde for 2 h. The samples were then rinsed with PBS and stained with 0.1% Sirius Red dissolved in saturated picric acid for 18 h. Following being washed with 0.1 M acetic acid, the stained samples were imaged under an optical microscope. For quantification, each stained sample was immersed in 1 mL of mixed solution containing 0.2 M NaOH and methanol (1:1) to elute the stain, and the optical density at 528 nm was measured.

2.14. Extracellular Matrix Mineralization Assay. The extracellular matrix mineralization was evaluated by SEM analysis and calcium content test. After culturing for 14 days, the cells on the samples were fixed, dehydrated in graded concentrations of ethanol, and dried in a freeze-dryer. Subsequently, the samples were sputtered with a thin platinum layer and observed under the SEM. To compare the calcium precipitation during the cell culture, we washed and soaked the samples in 1 M acetic acid overnight. The solution was

DOI: 10.1021/acsami.5b03172
ACS Appl. Mater. Interfaces 2015, 7, 14384−14396

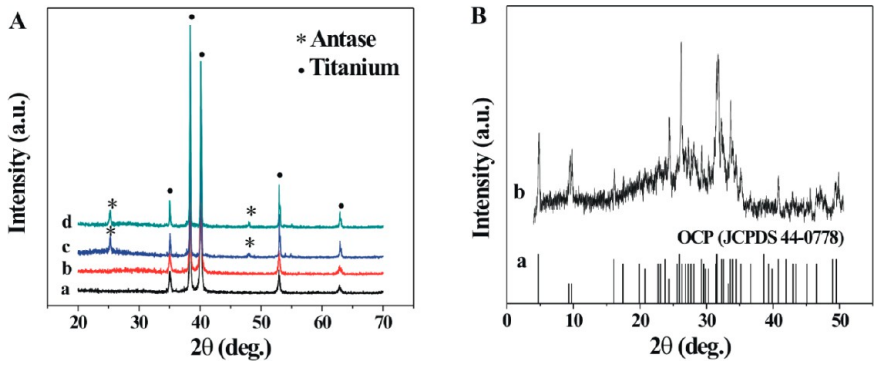

Figure 2. (A) XRD patterns of (a) PTi, (b) PTi−OCP, (c) MS-450, and (d) MS-450−OCP. (B) XRD patterns of (a) the reference data of OCP and (b) OCP powders.

then collected, and the absorbance was measured at 610 nm according to the calcium assay kit (Jiancheng Bioengineering Institute, China). Meanwhile, the calcium content of the OCP on the PTi−OCP and MS-450−OCP was measured as well to avoid interference.

2.15. Statistical Analysis. All of the data were collected from at least three samples for each group and expressed as mean values ± standard deviations (SD). Statistical comparisons were analyzed via one-way variance analysis (ANOVA) with SPSS 11.0 software, and a value of $p < 0.05$ was considered to be statistically significant.

3. RESULTS AND DISCUSSION

3.1. Morphology and Phase Analysis. The SEM micrographs of the various surfaces are shown in Figure 1. It is noted that small stripes appeared on the PTi surface via the surface polishing process, whereas a hierarchical structure consisting of a nanospongelike structure (ranging between 10−150 nm in pore size) uniformly distributed on the microporous titanium surface (diameter of 2−6 μm) was constructed on a pure titanium surface by the acid etching and anodization. After electrodeposition in a mixed CaP solution, a thin ribbonlike calcium phosphate coating was formed on the PTi and MS-450 surfaces. As shown in parts b, d, e, and g of Figure 1, the deposited OCP morphology was different on the different surface structures of Ti substrates (PTi or MS-450). On the MS-450−OCP surface, the OCP crystals nucleated and grew along the micro/nanostructured surface and partially covered the nanospongelike porous TiO_2, which actually increased the microscale perturbation, although it may modify the nanoscale features on the surface. It is found that the deposition of OCP on the MS-450 surface did not significantly influence the surface structure, which retained its rugged and wavelike morphology (Figure 1f,g) under the controlled electrodeposition conditions. However, the OCP on the plane substrate appeared to extend away from the surface to form a petal-shaped structure with a size of 100−800 nm (Figure 1e) using the same deposition method.

Table 1. Contact Angle (°) and Values of Surface Free Energy (mJ/m^2) of (a) PTi, (b) PTi−OCP, (c) MS-450, and (d) MS-450−OCP of Ti Samples

	contact angle (°)		.
	water	ethylene glycol	surface free energy (mJ/m^2)
a	57.7 ± 1.46	51.5 ± 1.71	46.82
b	19.9 ± 1.69	8.8 ± 1.65	79.02
c	≈0	≈0	88.00
d	5.9 ± 1.97	4.6 ± 1.01	87.35

The XRD analysis was performed to identify the crystal structure of the various surfaces, and the patterns are shown in Figure 2A. All of the samples yielded major α-phase titanium peaks, and the MS-450 as well as the MS-450−OCP of the Ti samples presented additional peaks of the anatase titania (25.2 and 48°).[22] However, diffraction peaks related to CaP were not detected on both PTi−OCP and MS-450−OCP, which was ascribed to the fact that the CaP coating was too thin to be detected. To determine the composition of the CaP, we scraped off the coating and analyzed the powders by XRD. As shown in Figure 2B, the diffraction peaks of CaP powders are comparable to the reference data (JCPDS 44-0778) from OCP. Thus, the XRD analysis confirms that the deposited CaP coating is mainly composed of OCP.

3.2. Hydrophilicity Measurement. Table 1 shows the hydrophilicity analysis of different substrates by the sessile drop method. On the basis of the contact angle values, we determined that the PTi surface displayed the largest water

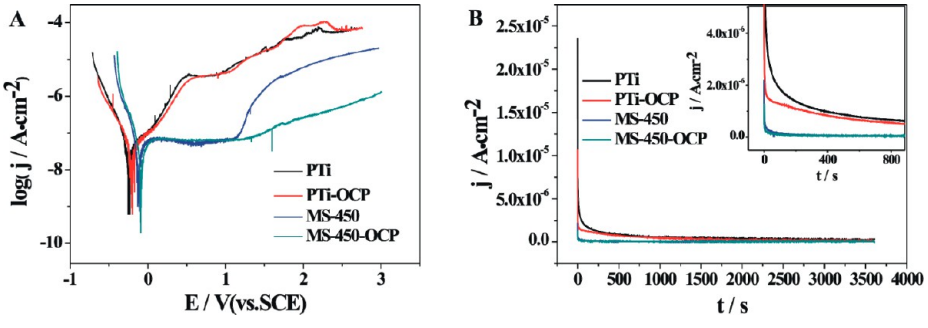

Figure 3. Electrochemical measurements of different Ti samples in PBS: (A) potentiodynamic polarization curves and (B) current-transient curves.

DOI: 10.1021/acsami.5b03172
ACS Appl. Mater. Interfaces 2015, 7, 14384−14396

Table 2. Electrochemical Polarization Parameters of Different Ti samples: (a) PTi, (b) PTi−OCP, (c) MS-450, and (d) MS-450−OCP

	a	b	c	d
E_{corr} (V vs SCE)	−0.241	−0.195	−0.120	−0.095
I_{corr} (A/cm^2)	3.663×10^{-8}	2.321×10^{-8}	1.742×10^{-8}	1.125×10^{-8}
j_{pass}(A/cm^2)	3.567×10^{-6}	3.467×10^{-6}	7.672×10^{-8}	7.058×10^{-8}

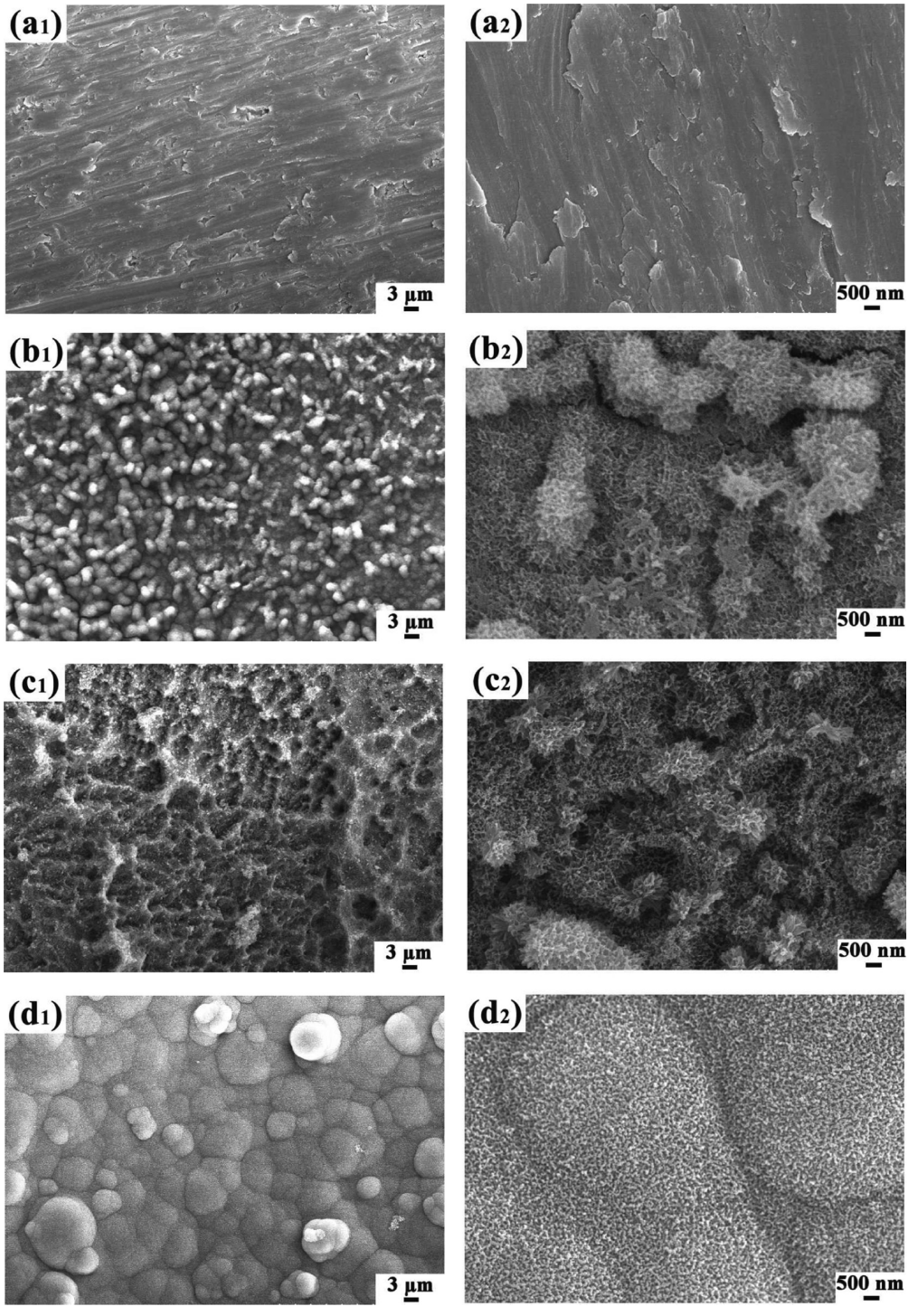

Figure 4. SEM micrographs of apatite precipitation after immersion in SBF on (a) PTi, (b) PTi−OCP, (c) MS-450, and (d) MS-450−OCP. Parts a_2−d_2 are high-magnification images of the samples in parts a_1−d_1, respectively.

contact angle among all the groups, with a value of 57.7°. The PTi−OCP presented a moderate value of 19.9°; however, the MS-450 and MS-450−OCP surfaces exhibited superhydrophilic properties, with contact angles of around 0° and 5.9°,

DOI: 10.1021/acsami.5b03172
ACS Appl. Mater. Interfaces 2015, 7, 14384−14396

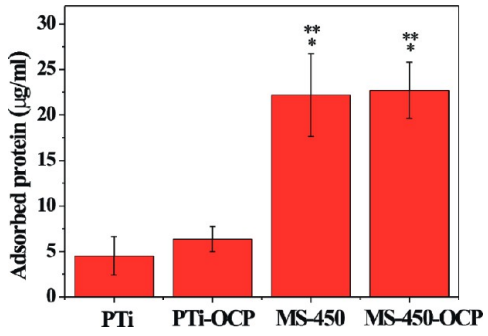

Figure 5. Amount of protein adsorption to different Ti samples: (a) PTi, (b) PTi−OCP, (c) MS-450, and (d) MS-450−OCP. Significance: *, $p < 0.05$ (compared with the adsorption in PTi) and **, $p < 0.05$ (compared with the adsorption in PTi−OCP).

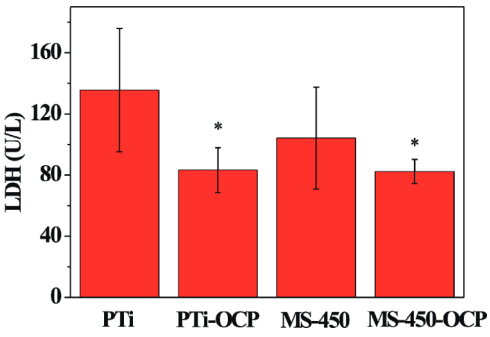

Figure 6. Assay of lactate dehydrogenase (LDH) activity of the culture medium after a 24 h incubation of cells on different Ti samples. Significance: *, $p < 0.05$ (compared with the activity in PTi).

respectively. The corresponding surface energy of the different Ti samples was obtained according to the Owens−Wendt (OW) method.[23] It is noteworthy that the surface energy of the treated surfaces increased significantly after the surface modification of the PTi surfaces. The MS-450 and MS-450−OCP yielded much higher surface energy values (88.0 and 87.35 mJ/m^2, respectively) compared to those of PTi−OCP (79.02 mJ/m^2) and PTi (46.82 mJ/m^2). In brief, the wettability and surface energy of the treated surfaces are dramatically enhanced, although the enhanced extent is different.

3.3. Corrosion Resistance. Figure 3A presents the potentiodynamic polarization curves of various samples in the PBS solution and the corresponding corrosion parameter values, such as corrosion potential (E_{corr}), corrosion current density (I_{corr}) and passive current density (j_{pass}), are listed in Table 2. The E_{corr} values obtained from the PTi−OCP shifted slightly to the noble direction in comparison to that of the PTi, and a more significant potential shift was detected from the MS-450 and MS-450−OCP. The MS-450−OCP achieved the lowest values of corrosion current density (I_{corr}), but there was no obvious variation of I_{corr} among all the groups. However, as can be seen from the polarization curves, the MS-450 and MS-450−OCP exhibited much lower values of passive current density, with j_{pass} values of 7.672×10^{-8} and 7.058×10^{-8} A/cm^2, respectively. The lower j_{pass} and the broader passive regions mean higher resistance to corrosion for the metallic substrates after oxidation and OCP modification.[24]

Chrono-amperometric measurements, with an external applied potential of 0.5 V (versus SCE), were performed to further illustrate the surface electrochemical behaviors of the different Ti samples. As shown in Figure 3B, overall the current-transient curves suggested that all the samples exhibited a high current density value at the initial immersion stage, and it then decreased significantly and finally reached a plateau after a short term. In the cases of PTi and PTi−OCP, the current density values were as high as 2.36×10^{-5} and 1.07×10^{-5} A/cm^2, respectively, at the initial stage. As the immersion time increased, the above current density values sharply decreased to 1.45×10^{-6} and 1.13×10^{-6} A/cm^2, respectively, after 180 s and then reached plateau values of 5.65×10^{-7} and 4.07×10^{-7} A/cm^2, respectively. As to the MS-450 and MS-450−OCP, the current density values were 2.2×10^{-6} and 1.28×10^{-6} A/cm^2 at the initial stage; afterward, similar plateau current density values (around 5.87×10^{-8} A/cm^2) were measured, indicating that a much lower corrosion rate occurred in the physiological solution when compared to those of the PTi and PTi−OCP. The polarization and chrono-amperometric measurements indicate that the formation of anatase TiO_2 and OCP films is able to enhance the chemical stability and corrosion resistance of Ti substrates, which is important for the long-term biocompatibility of metallic implants.

3.4. Apatite-Forming Ability. Figure 4 displays the SEM micrographs of the different Ti samples after soaking in SBF. Obviously, different apatite precipitate behaviors of various titanium surfaces were observed. A small quantity of ball-like particles appeared on the MS-450 surface, in contrast to the fact that no precipitate was deposited on the PTi surface. However, as for PTi−OCP and MS-450−OCP, both of the surfaces were completely covered by apatite precipitates, and remarkably, a much denser and thicker CaP precipitate layer was observed on the MS-450−OCP.

There are many factors causing the apatite nucleation and precipitation, such as surface morphology,[22] surface wettability,[25] and surface charge.[26] It is well-accepted that when immersed in SBF, the enhanced surface wettability of Ti surfaces benefits the hydroxylation of titania to form Ti−OH groups,[25] which is important for the nucleation process. Because the isoelectric point of TiO_2 is 5−6 under neutral pH conditions and the pH environment of SBF is around 7.40, the Ti−OH groups on the surface are negatively charged and then selectively attract the positively charged Ca^{2+} cations.[27] With the increased amount of Ca^{2+} cations, the surface becomes positively charged and subsequently adsorbs negatively charged PO_4^{3-} anions to form apatite nuclei for further apatite precipitation.[25,27] However, it is noticeable that the apatite-inducing ability on the MS-450−OCP was significantly enhanced in comparison to that of the MS-450, which is attributed to the contribution of the OCP thin layer. The OCP, mainly consisting of Ca^{2+} and PO_4^{3-}, is able to reduce the incubation time needed for the enhancement of the localized aggregation of Ca^{2+} and PO_4^{3-} and probably enriches the surface with more nucleation sites for apatite precipitation. Additionally, it is noted that the PTi−OCP showed a better apatite-inducing ability than the MS-450, suggesting that the OCP layer plays a more dominant role in apatite formation over the surface morphology and wettability. In brief, the enhanced bonelike apatite growth rate on the MS-450−OCP results from the synergistic effect of the combination of the micro/nano hybrid structure and the OCP thin layer.

3.5. Protein Adsorption. It is suggested that protein adsorption onto the implant surface is an important process in determining the biocompatibility because the adsorbed protein has a vital influence on the response of cells to the biomaterials.[4,28] Thus, the amount of protein adsorption on

DOI: 10.1021/acsami.5b03172
ACS Appl. Mater. Interfaces 2015, 7, 14384−14396

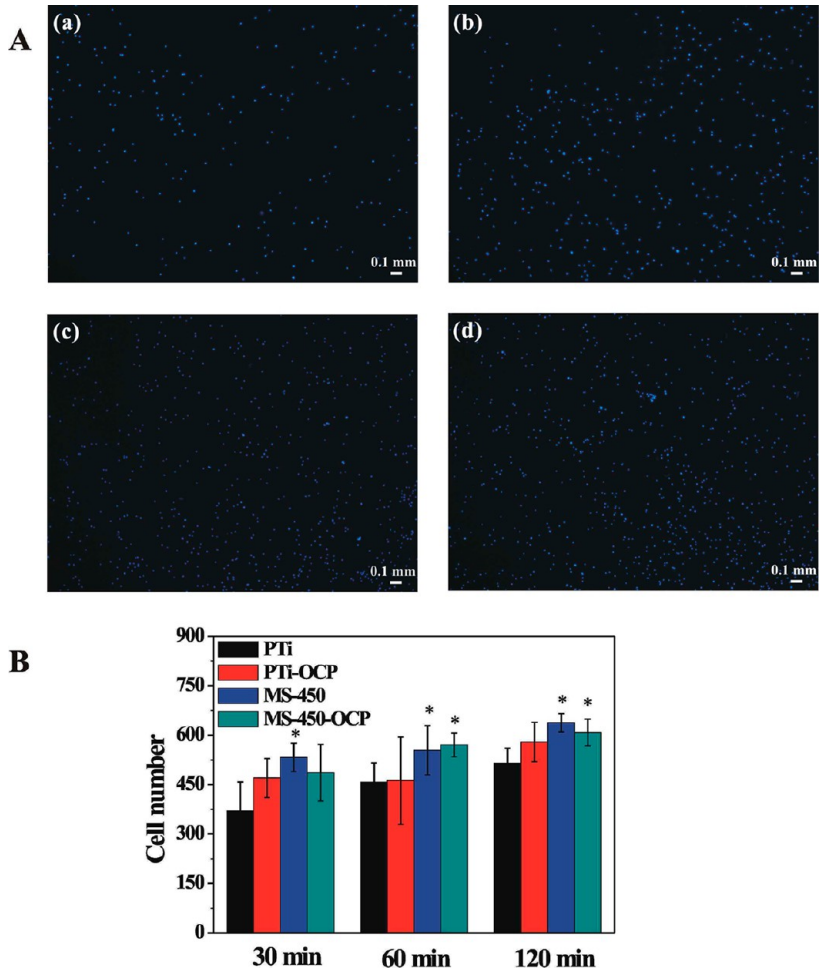

Figure 7. (A) Fluorescence microscopy images of DAPI-stained cells adhered to different Ti samples: (a) PTi, (b) PTi−OCP, (c) MS-450, and (d) MS-450−OCP. (B) The quantitative results of cell numbers. Significance: *, $p < 0.05$ (compared with the cell number in PTi).

the prepared surfaces was assayed, and the results are displayed in Figure 5. It is evident that more protein (by nearly a factor of 3) adsorbed on the MS-450 and MS-450−OCP than did the protein on the PTi and PTi−OCP, although no obvious difference of protein adsorption was detected between the MS-450 and MS-450−OCP. The increased protein adsorption is mainly attributed to the existence of the micro/nanostructure, which provides a higher specific surface area for enhancing the efficiency and capacity of protein anchoring and adsorption, whereas the OCP coating is too thin to greatly influence the amount of protein adsorption on the MS-450 and MS-450−OCP.

3.6. Cytotoxicity Assay. The cytotoxicity of the prepared samples was indicated by assaying the lactate dehydrogenase (LDH) release of MC3T3-E1 into the culture medium after 24 h of incubation, and the LDH activity is compared in Figure 6. It is noted that MS-450 presented a slightly lower cytotoxicity than the PTi, but the statistical difference was not significant. However, the existence of OCP on the PTi−OCP and MS-450−OCP surfaces significantly lowered the cytoxicity level compared to that of the PTi surface, indicating that the deposition of OCP and the surface modification of titanium are able to reduce the cytotoxicity of the blank Ti surface.

3.7. Cell Adhesion. The cell adhesion on the substrates during the initial 2 h of culturing was observed by DAPI staining, and the numbers were counted. As shown in Figure 7, when the incubation was prolonged from 30 to 120 min, the amount of cells adhered to the substrates gradually increased, and almost all of the treated samples had more adherent cells on the surfaces than did the PTi at each time interval, but there were no statistical differences observed among the three treated groups during such a 2 h period. It is obvious that more cells appeared on the MS-450 than those on the PTi, with a statistical difference at 30 min; however, no significant differences were detected among the PTi, PTi−OCP, and MS-450−OCP. After 60 and 120 min of incubation, the cell numbers on the MS-450 and MS-450−OCP samples were obviously higher than those on the PTi, while the statistical difference of cell numbers between the PTi and PTi−OCP samples were not significant. At 120 min, the numbers of adherent cells on the PTi−OCP, MS-450, and MS-450−OCP appeared to be higher by 13%, 24%, and 18%, respectively, than that on the PTi.

3.8. Cell Morphology. Figure 8 shows the morphology of cells after 1 day of incubation on the various samples. The spread of cells was remarkably regulated by the different constructed surfaces. It is noted that cells spread out with a fusiform shape along the polishing scratches on the PTi, and a small amount of filopodia was stretched out. By contrast, cells on the PTi−OCP, MS-450, and MS-450−OCP displayed a polygonal shape with prominent filopodia and lamellipodia protrusions. The treated surfaces are able to modulate the cells

DOI: 10.1021/acsami.5b03172
ACS Appl. Mater. Interfaces 2015, 7, 14384−14396

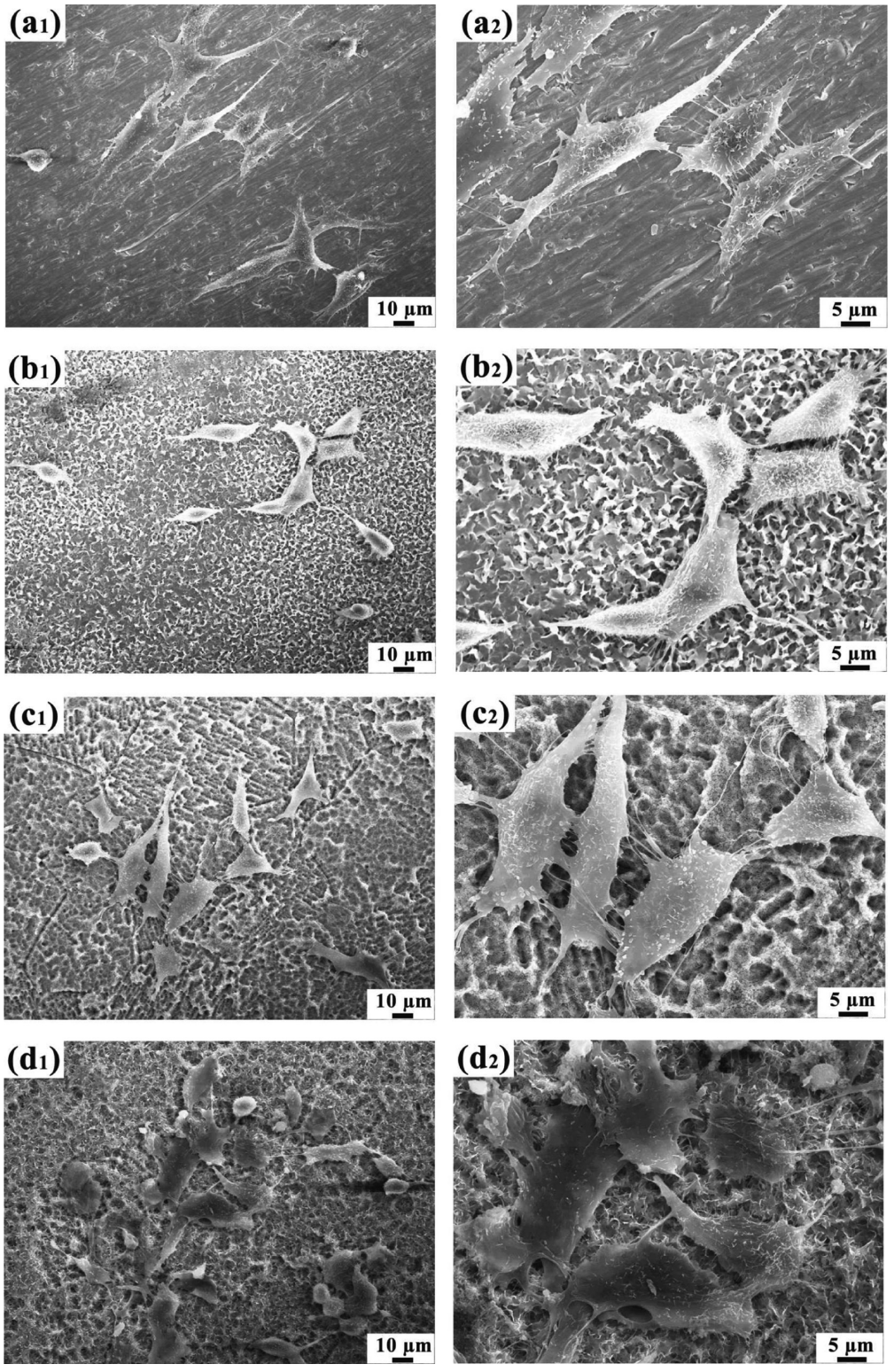

Figure 8. Cell morphology after a 24 h incubation on different Ti samples: (a) PTi, (b) PTi-OCP, (c) MS-450, and (d) MS-450-OCP. Parts a_2−d_2 are high-magnification images of the samples in parts a_1−d_1, respectively.

to be more stereoscopic and extended than the PTi surface; in particular, MS-450 and MS-450−OCP surfaces dramatically promote cell extension and make the cells to bridge over the concave areas via the cell podia.

3.9. Cell Proliferation. Cell proliferation on the different surfaces was determined by MTT metabolic assay, and the results are shown in Figure 9. It is obvious that the MC3T3-E1 cells proliferated significantly on every group during the culture period. After 1 day of culturing, there were no significant differences among all of the groups. For 4 days of culturing, the cell numbers on the MS-450 and MS-450−OCP surfaces were much higher than those on the PTi and PTi−OCP surfaces, but the difference between the former results was negligible. At day seven, the highest cell number was discerned on the MS-450−

DOI: 10.1021/acsami.5b03172
ACS Appl. Mater. Interfaces 2015, 7, 14384−14396

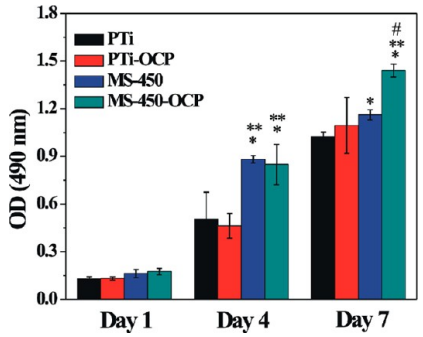

Figure 9. MTT assay of cells cultured on different Ti samples for 1, 4, and 7 days. Significance is indicated by *, $p < 0.05$ (compared with the values on PTi); **, $p < 0.05$ (compared with the values on PTi−OCP); and #, $p < 0.05$ (compared with the values on MS-450).

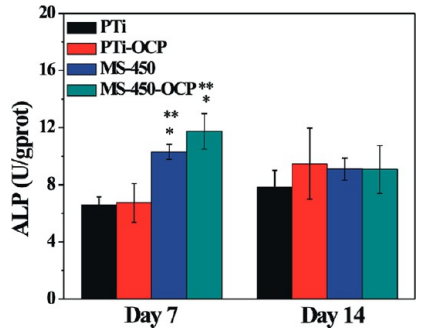

Figure 10. ALP activity of cells cultured on different Ti samples for 7 and 14 days. Significance: *, $p < 0.05$ (compared with the activity of PTi) and **, $p < 0.05$ (compared with the activity of PTi−OCP).

OCP surface and followed by that on the MS-450. Although PTi−OCP showed a higher cell number than that on the PTi surface, the statistical difference was not significant.

Several previous studies have shown that the existence of microstructured roughness reduces the cell proliferation in contrast to that on blank Ti surfaces,[29−31] and the nanostructured roughness added to the microstructured surface may achieve an enhanced proliferation compared to that on the microstructured surface or even slightly higher than that on the blank Ti surface.[14] Although the different types of cells should be taken into account, it is generally believed that the cells sense the substrates via integrin clustering to form focal contact to induce cell adhesion and proliferation.[32−34] Park et al. found that a nanotube surface with a diameter of 30−50 nm represented a critical borderline for favorable cell attachment and growth.[34] Arnold et al. showed that a separation of 58−73 nm between gold nanodots was a universal length scale for integrin clustering and focal adhesion formation.[35] The superior cell proliferation of MS-450 and MS-450−OCP surfaces may be attributed to heterogeneous nanoscale sizes on the microporous surface providing a multilevel scale for integrin formation and activation to induce cell adhesion and proliferation. Additionally, the surface wettability influences the cell viability.[36] Although the optimal range of surface wettability and energy still needs to be considered because it is difficult to focus on the effect of surface wettability on osteoblasts without altering the surface topography and composition, some reports have shown that the enhanced wettability is beneficial to cell attachment and proliferation.[37,38] In short, the best cell proliferation on the MS-450−OCP is due to the comprehensive results of surface structure, composition, and wettability. The enhanced cell proliferation is favorable because high cell proliferation signifies that more cells colonize the implant surface, probably resulting in greater bone mass accumulated when implanted in vivo, thus ensuring better bone−implant bonding.

3.10. Alkaline Phosphatase Activity. The ALP activity at days 7 and 14 was measured, and the results are displayed in Figure 10. It is obvious that the ALP activity at day 7 on the MS-450 and MS-450−OCP was significantly promoted by 55% and 75% relative to that on the PTi and PTi−OCP; moreover, the ALP activity on the MS-450−OCP was determined to be slightly higher than that on the MS-450, but the statistical difference was not obvious. After 14 days of cell culturing, the ALP activity on the MS-450 and MS-450−OCP decreased in comparison to that at day 7; however, the ALP activity on the PTi and PTi−OCP appeared to be increased, but the increase was not statistically significant. Finally, all of the treated samples achieved a slightly higher ALP activity than the PTi, even though there were no appreciable differences among all the groups.

The activity of ALP is widely regarded as an early stage marker associated with the differentiation potential of osteoblasts.[39] The increased ALP activity on the PTi and PTi−OCP from day 7 to day 14 is ascribed to the continuous osteoblast differentiation; however, the decreased ALP activity on the MS-450 and MS-450−OCP during the same period is probably related to the osteoblasts entering the mineralization stage.[39]

3.11. Collagen Secretion. Collagen production was evaluated and quantified by Sirius Red staining. As shown in Figure 11, it is noted that more collagen was secreted by the cells on the PTi−OCP, MS-450, and MS-450−OCP compared to that from PTi at day 7; also, much denser collagen was deposited on the MS-450 and MS-450−OCP than that on the PTi−OCP. According to the quantitative results, the collagen production was increased by 19%, 86%, and 89% on the PTi−OCP, MS-450, and MS-450−OCP compared to that on the PTi, respectively. When the cell incubation was prolonged to 14 days, the amount of collagen secreted on all of the groups was significantly increased in comparison to the amount at day 7. It is observed that the MS-450−OCP displayed the most collagen production among all of the groups, almost 50% more than that on the PTi. It is generally accepted that collagen is the major secreted product during cell culture,[39] and the formation of collagenous matrix, in turn, contributes to osteoblast differentiation and renders the matrix competent for mineralization.[39,40]

3.12. Extracellular Matrix Mineralization. The extracellular matrix mineralization was compared by observing the cell morphology and determining the amount of calcium deposition after 14 days of incubation. As shown in Figure 12, the cells with collagen fibers spread well on all the substrates. It is noteworthy that calcium nodules appeared on the PTi−OCP, MS-450, and MS-450−OCP, in comparison to having none observed on the PTi. According to the quantitative analysis (Figure 13), MS-450−OCP presented the highest calcium content among all the groups, and it was markedly promoted by 53% compared to the amount in PTi. As to the PTi−OCP and MS-450, the amount of calcium formed on them was similar, and it was enhanced by 33% in comparison with that on the PTi.

It is noted that ALP activity, collagen secretion, and extracellular matrix mineralization were drastically enhanced

DOI: 10.1021/acsami.5b03172
ACS Appl. Mater. Interfaces 2015, 7, 14384−14396

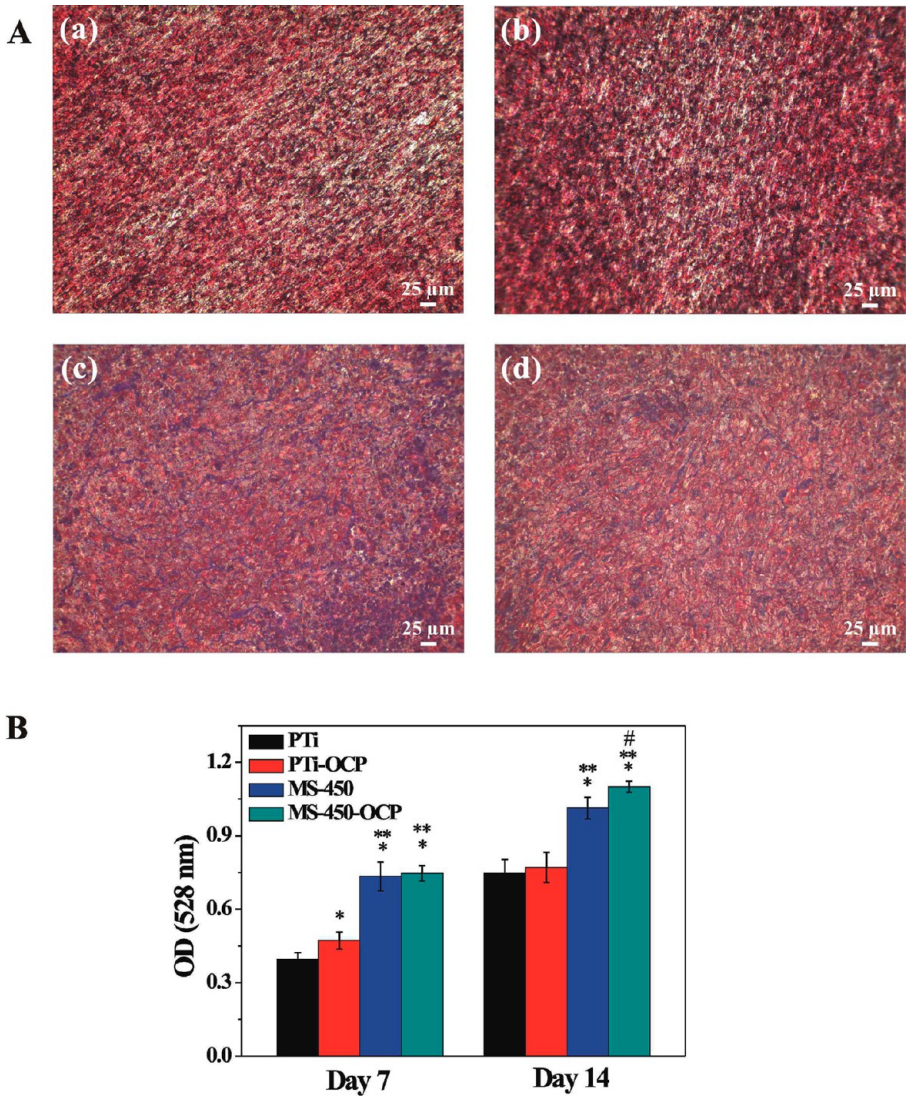

Figure 11. (A) Staining of collagen secreted by cells on different Ti samples: (a) PTi, (b) PTi−OCP, (c) MS-450, and (d) MS-450−OCP. (B) The quantitative results of collagen secretion by colorimetric analysis. Significance is indicated by *, $p < 0.05$ (compared with the values in PTi); **, $p < 0.05$ (compared with the values in PTi−OCP); and #, $p < 0.05$ (compared with the values in MS-450).

on the MS-450 and MS-450−OCP, being especially obvious on the MS-450−OCP. The reasons are mainly ascribed to the surface structure and composition. It is reported that a combination of microscale and nanoscale features has a distinct influences on osteoblast differentiation and mineralization.[14,15] Zhao et al. added an array of TiO_2 nanotubes with a diameter of 25 or 80 nm on the micropitted topography, and they found that the micro/nanotextured surface achieved an equivalent or even enhanced ALP activity, extracellular matrix deposition, and mineralization than that on the polished titanium surface.[14] Kubo et al. added 200 nm TiO_2 nanonodules to the micropitted surface and observed that such a micro/nano hybrid surface greatly enhanced the ALP activity, the subsequent gene expressions (osteopontin and osteocalcin), and the mineralizing activity.[15] Although such results are promising, it is still necessary to systematically investigate and optimize the surface properties without greatly compromising the superior bioactivity of the hierarchical hybrid structure. Our construction of the micro/nano structured surface is able to promote osteoblast differentiation and mineralization, which results from the multilevel surface features consisting of micro- and nanoscale roughness that may provide a synergistic effect on cell−cell communication and the activation of signaling pathways controlling cell differentiation and mineralization. Furthermore, previous studies have shown that OCP possesses a positive stimulatory effect on cell differentiation. According to Suzuki et al.,[41] mouse bone marrow stromal ST-2 cells were incubated on the OCP-coated tissue culture plates, and it was found that OCP was capable of boosting cell differentiation even without the addition of osteogenic supplements. Other in vivo tests also showed that OCP-coated porous tantalum or dense titanium cylinders was able to stimulate bone formation in contrast to formation on bare ones,[42] and pure OCP implants effectively induced new bone formation when implanted in mouse calvaria.[11] Even though the exact mechanism of the OCP stimulation of cell differentiation and mineralization is still undetermined, it is commonly believed that OCP is osteoconductive and bioactive, thus securing the stimulatory influence on osteogenesis.[9] Additionally, the enhanced wettability of the constructed surfaces also contributes to the osteoblast responses. Lim et al. observed the increased differentiation and mineral deposition of hFOB

DOI: 10.1021/acsami.5b03172
ACS Appl. Mater. Interfaces 2015, 7, 14384−14396

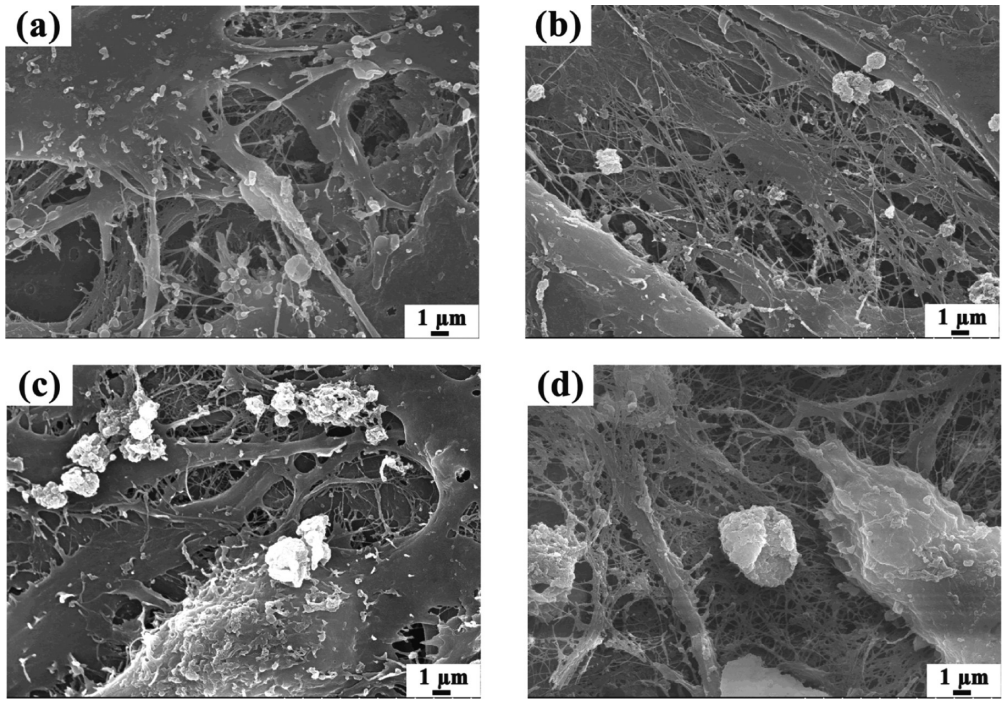

Figure 12. SEM micrographs of cell morphology on different Ti samples after incubation for 14 days: (a) PTi, (b) PTi−OCP, (c) MS-450, and (d) MS-450−OCP.

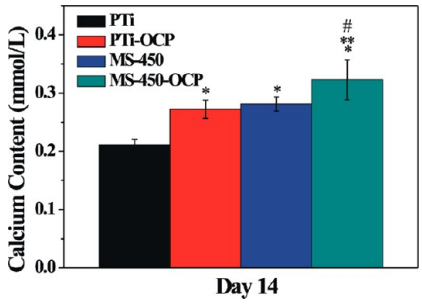

Figure 13. Amounts of calcium deposited on different Ti samples by cells after culture for 14 days. Significance indicated by *, $p < 0.05$ (compared with the amount in PTi); **, $p < 0.05$ (compared with the amount in PTi−OCP); and #, $p < 0.05$ (compared with the amount in MS-450).

cells on the hydrophilic quartz in contrast to cells on the hydrophobic surfaces.[43] Zhao et al. obtained a strong synergistic effect between surface roughness and surface energy on the MG63 cell differentiation on micron- and submicron-scale structured titanium surfaces.[44] Although there are no precisely defined roles of surface wettability and energy in influencing medium- or long-term cell functions, it is generally accepted that the increased surface wettability and energy tend to benefit cellular activities in vitro and osteogesis in vivo.[36] Thus, taken together, the superior cell differentiation and mineralization behaviors discerned on the MS-450−OCP is mainly due to the synergistic contribution of the micro/nano structure and OCP stimulatory effects, and the enhanced wettability is also favorable. It is generally believed that a mineralized extracellular matrix benefits osteoblasts differentiating into osteocytes, with the terminally differentiated cells surrounded by a mineralized matrix.[39,40,45] Subsequently, the bonelike nodules further undergo growth and accumulation to a bone-tissue-like organization.[39] Hence, such a construction of an OCP-induced micro/nanospongelike structured surface is promising for promoting bone regeneration when implanted in bone tissue.

4. CONCLUSIONS

In this study, a thin OCP coating was successfully deposited on the prepared micro/nanospongelike titania surface to form a combined hierarchical hybrid structure without greatly influencing the original micro/nano roughness, surface wettability, and surface energy. Such a hybrid structure displayed not only excellent corrosion resistance and chemical stability in physiological solution but also superior apatite-inducing ability. It is evident that the MC3T3-E1 cells showed much better adhesion, proliferation, and expression of alkaline phosphatase and extracellular matrix mineralization on the OCP-deposited micro/nanospongelike structured surface. From the cellular activity evaluations, it is concluded that the addition of an OCP thin layer to the micro/nanostructure presents a synergistic effect on osteoblast response with nearly all of the cell functions enhanced, which provides a promising strategy for improving the bioactivity as well as the osteointegration when implanted in vivo and consequently reduces wound healing time in clinical applications.

AUTHOR INFORMATION

Corresponding Authors

*C.L. Tel: +86 592 2189354. Fax: +86 592 2186657. E-mail: cjlin@xmu.edu.cn.

*P.T. Tel: +86-10-66938101. Fax: +86-10-6816-1218. E-mail: pftang301@163.com.

Notes

The authors declare no competing financial interest.

DOI: 10.1021/acsami.5b03172
ACS Appl. Mater. Interfaces 2015, 7, 14384−14396

■ ACKNOWLEDGMENTS

This work was supported by the Natural Science Foundation of China (21321062, 31370947, and 81171690), and the National Scientific Support Program of China (2012BAI07B09).

■ REFERENCES

(1) Liu, X.; Chu, P. K.; Ding, C. Surface modification of titanium, titanium alloys, and related materials for biomedical applications. *Mater. Sci. Eng., R* **2004**, *47*, 49−121.
(2) Shen, X.; Hu, Y.; Xu, G.; Chen, W.; Xu, K.; Ran, Q.; Ma, P.; Zhang, Y.; Li, J.; Cai, K. Regulation of the Biological Functions of Osteoblasts and Bone Formation by Zn-Incorporated Coating on Microrough Titanium. *ACS Appl. Mater. Interfaces* **2014**, *6*, 16426−16440.
(3) Liu, X.; Chu, P. K.; Ding, C. Surface Nanofunctionalization of Biomaterials. *Mater. Sci. Eng., R.* **2010**, *70*, 275−302.
(4) Huang, Q.; Lin, L.; Yang, Y.; Hu, R.; Vogler, E. A.; Lin, C. Role of Trapped Air in the Formation of Cell-and-Protein Micropatterns on Superhydrophobic/Superhydrophilic Microtemplated Surfaces. *Biomaterials* **2012**, *33*, 8213−8220.
(5) Cao, H.; Liu, X.; Meng, F.; Chu, P. K. Biological Actions of Silver Nanoparticles Embedded in Titanium Controlled by Microgalvanic Effects. *Biomaterials* **2011**, *32*, 693−705.
(6) Zhang, Q. Y.; Leng, Y.; Lu, X.; Xin, R. L.; Yang, X. D.; Chen, J. Y. Bioactive Films on Metallic Surfaces for Osteoconduction. *J. Biomed. Mater. Res., Part A* **2009**, *88*, 481−490.
(7) Poh, C. K.; Shi, Z.; Lim, T. Y.; Neoh, K. G.; Wang, W. The Effect of VEGF Functionalization of Titanium on Endothelial Cells in Vitro. *Biomaterials* **2010**, *31*, 1578−1585.
(8) Peterson, A. M.; Pilz-Allen, C.; Kolesnikova, T.; Möhwald, H.; Shchukin, D. Growth Factor Release from Polyelectrolyte-Coated Titanium for Implant Applications. *ACS Appl. Mater. Interfaces* **2013**, *6*, 1866−1871.
(9) LeGeros, R. Z. Calcium Phosphate-Based Osteoinductive Materials. *Chem. Rev.* **2008**, *108*, 4742−4753.
(10) Dekker, R. J.; de Bruijn, J. D.; Stigter, M.; Barrere, F.; Layrolle, P.; van Blitterswijk, C. A. Bone Tissue Engineering on Amorphous Carbonated Apatite and Crystalline Octacalcium Phosphate-Coated Titanium Discs. *Biomaterials* **2005**, *26*, 5231−5239.
(11) Kikawa, T.; Kashimoto, O.; Imaizumi, H.; Kokubun, S.; Suzuki, O. Intramembranous Bone Tissue Response to Biodegradable Octacalcium Phosphate Implant. *Acta Biomater.* **2009**, *5*, 1756−1766.
(12) Suzuki, O. Octacalcium Phosphate: Osteoconductivity and Crystal Chemistry. *Acta Biomater.* **2010**, *6*, 3379−3387.
(13) Rho, J.-Y.; Kuhn-Spearing, L.; Zioupos, P. Mechanical Properties and the Hierarchical Structure of Bone. *Med. Eng. & Phys.* **1998**, *20*, 92−102.
(14) Zhao, L.; Mei, S.; Chu, P. K.; Zhang, Y.; Wu, Z. The Influence of Hierarchical Hybrid Micro/Nano-textured Titanium Surface with Titania Nanotubes on Osteoblast Functions. *Biomaterials* **2010**, *31*, 5072−5082.
(15) Hori, N.; Iwasa, F.; Ueno, T.; Takeuchi, K.; Tsukimura, N.; Yamada, M.; Hattori, M.; Yamamoto, A.; Ogawa, T. Selective Cell Affinity of Biomimetic Micro-Nano-Hybrid Structured TiO_2 Overcomes the Biological Dilemma of Osteoblasts. *Dent. Mater.* **2010**, *26*, 275−287.
(16) Gittens, R. A.; McLachlan, T.; Olivares-Navarrete, R.; Cai, Y.; Berner, S.; Tannenbaum, R.; Schwartz, Z.; Sandhage, K. H.; Boyan, B. D. The Effects of Combined Micron-/Submicron-Scale Surface Roughness and Nanoscale Features on Cell Proliferation and Differentiation. *Biomaterials* **2011**, *32*, 3395−3403.
(17) Liu, Q.; Wang, W.; Zhang, L.; Zhao, L.; Song, W.; Duan, X.; Zhang, Y. Involvement of N-Cadherin/β-Catenin Interaction in the Micro/Nanotopography Induced Indirect Mechanotransduction. *Biomaterials* **2014**, *35*, 6206−6218.
(18) Gittens, R. A.; Olivares-Navarrete, R.; Cheng, A.; Anderson, D. M.; McLachlan, T.; Stephan, I.; Geis-Gerstorfer, J.; Sandhage, K. H.; Fedorov, A. G.; Rupp, F.; Boyan, B. D.; Tannenbaum, R.; Schwartz, Z. The Roles of Titanium Surface Micro/Nanotopography and Wettability on the Differential Response of Human Osteoblast Lineage Cells. *Acta Biomater.* **2013**, *9*, 6268−6277.
(19) Lai, Y. K.; Lin, C. J.; Wang, H.; Huang, H. Y.; Zhuang, H. F.; Sun, L. Superhydrophilic−Superhydrophobic Micropattern on TiO_2 Nanotube Films by Photocatalytic Lithography. *Electrochem. Commun.* **2008**, *10*, 387−391.
(20) Narayanan, R.; Seshadri, S. K. Point Defect Model and Corrosion of Anodic Oxide Coatings on Ti−6Al−4V. *Corros. Sci.* **2008**, *50*, 1521−1529.
(21) Kokubo, T.; Takadama, H. How Useful is SBF in Predicting in Vivo Bone Bioactivity? *Biomaterials* **2006**, *27*, 2907−2915.
(22) Kunze, J.; Müller, L.; Macak, J. M.; Greil, P.; Schmuki, P.; Müller, F. A. Time-Dependent Growth of Biomimetic Apatite on Anodic TiO_2 Nanotubes. *Electrochim. Acta* **2008**, *53*, 6995−7003.
(23) Wang, Y.; Wen, C.; Hodgson, P.; Li, Y. Biocompatibility of TiO_2 Nanotubes with Different Topographies. *J. Biomed. Mater. Res., Part A* **2013**, *102*, 743−751.
(24) Alves, V. A.; Reis, R. Q.; Santos, I. C. B.; Souza, D. G.; de F. Gonçalves, T.; Pereira-da-Silva, M. A.; Rossi, A.; da Silva, L. A. In Situ Impedance Spectroscopy Study of the Electrochemical Corrosion of Ti and Ti−6Al−4V in Simulated Body Fluid at 25 and 37 °C. *Corros. Sci.* **2009**, *51*, 2473−2482.
(25) Tavangar, A.; Tan, B.; Venkatakrishnan, K. Synthesis of Bio-Functionalized Three-Dimensional Titania Nanofibrous Structures Using Femtosecond Laser Ablation. *Acta Biomater.* **2011**, *7*, 2726−2732.
(26) Kokubo, T.; Pattanayak, D. K.; Yamaguchi, S.; Takadama, H.; Matsushita, T.; Kawai, T.; Takemoto, M.; Fujibayashi, S.; Nakamura, T. Positively Charged Bioactive Ti Metal Prepared by Simple Chemical and Heat Treatments. *J. R. Soc., Interface* **2010**, *7*, S503−S513.
(27) Cui, X. Y.; Kim, H. M.; Kawashita, M.; Wang, L. B.; Xiong, T. Y.; Kokubo, T.; Nakamura, T. Effect of Hot Water and Heat Treatment on the Apatite-Forming Ability of Titania Films Formed on Titanium Metal via Anodic Oxidation in Acetic Acid Solutions. *J. Mater. Sci.: Mater. Med.* **2008**, *19*, 1767−1773.
(28) Vogler, E. A. Protein Adsorption in Three Dimensions. *Biomaterials* **2012**, *33*, 1201−1237.
(29) Saito, T.; Hayashi, H.; Kameyama, T.; Hishida, M.; Nagai, K.; Teraoka, K.; Kato, K. Suppressed Proliferation of Mouse Osteoblast-Like Cells by a Rough-Surfaced Substrate Leads To Low Differentiation And Mineralization. *Mater. Sci. Eng., C* **2010**, *30*, 1−7.
(30) Boyan, B. D.; Lossdoerfer, S.; Wang, L.; Zhao, G.; Lohmann, C. H.; Cochran, D. L.; Schwartz, Z. Osteoblasts Generate an Osteogenic Microenvironment When Grown on Surfaces with Rough Microtopographies. *Eur. Cells Mater.* **2003**, *6*, 22−27.
(31) Kim, M.-J.; Kim, C.-W.; Lim, Y.-J.; Heo, S.-J. Microrough titanium surface affects biologic response in MG63 osteoblast-like cells. *J. Biomed. Mater. Res., Part A* **2006**, *79*, 1023−1032.
(32) Schlaepfer, D. D.; Hauck, C. R.; Sieg, D. J. Signaling through Focal Adhesion Kinase. *Prog. Biophys. Mol. Biol.* **1999**, *71*, 435−478.
(33) DeMali, K. A.; Wennerberg, K.; Burridge, K. Integrin Signaling to the Actin Cytoskeleton. *Curr. Opin. Cell Biol.* **2003**, *15*, 572−582.
(34) Park, J.; Bauer, S.; von der Mark, K.; Schmuki, P. Nanosize and Vitality: TiO_2 Nanotube Diameter Directs Cell Fate. *Nano Lett.* **2007**, *7*, 1686−1691.
(35) Arnold, M.; Cavalcanti-Adam, E. A.; Glass, R.; Blümmel, J.; Eck, W.; Kantlehner, M.; Kessler, H.; Spatz, J. P. Activation of Integrin Function by Nanopatterned Adhesive Interfaces. *ChemPhysChem* **2004**, *5*, 383−388.
(36) Gittens, R. A.; Scheideler, L.; Rupp, F.; Hyzy, S. L.; Geis-Gerstorfer, J.; Schwartz, Z.; Boyan, B. D. A Review on the Wettability of Dental Implant Surfaces II: Biological and Clinical Aspects. *Acta Biomater.* **2014**, *10*, 2907−2918.
(37) Park, J. W.; Kim, Y. J.; Jang, J. H.; Kwon, T. G.; Bae, Y. C.; Suh, J. Y. Effects of Phosphoric Acid Treatment of Titanium Surfaces on Surface Properties, Osteoblast Response and Removal of Torque Forces. *Acta Biomater.* **2010**, *6*, 1661−1670.

DOI: 10.1021/acsami.5b03172
ACS Appl. Mater. Interfaces 2015, 7, 14384−14396

(38) Liu, X. M.; Lim, J. Y.; Donahue, H. J.; Dhurjati, R.; Mastro, A. M.; Vogler, E. A. Influence of Substratum Surface Chemistry/Energy and Topography on the Human Fetal Osteoblastic Cell Line hFOB 1.19: Phenotypic and Genotypic Responses Observed in Vitro. *Biomaterials* **2007**, *28*, 4535−4550.
(39) Lian, J. B.; Stein, G. S. Concepts of Osteoblast Growth and Differentiation: Basis for Modulation of Bone Cell Development and Tissue Formation. *Crit. Rev. Oral Biol. Med.* **1992**, *3*, 269−305.
(40) Owen, T. A.; Aronow, M.; Shalhoub, V.; Barone, L. M.; Wilming, L.; Tassinari, M. S.; Kennedy, M. B.; Pockwinse, S.; Lian, J. B.; Stein, G. S. Progressive Development of the Rat Osteoblast Phenotype in Vitro: Reciprocal Relationships in Expression of Genes Associated with Osteoblast Proliferation and Differentiation during Formation of the Bone Extracellular Matrix. *J. Cell Physiol.* **1990**, *143*, 420−430.
(41) Suzuki, O.; Kamakura, S.; Katagiri, T.; Nakamura, M.; Zhao, B.; Honda, Y.; Kamijo, R. Bone Formation Enhanced by Implanted Octacalcium Phosphate Involving Conversion into Ca-Deficient Hydroxyapatite. *Biomaterials* **2006**, *27*, 2671−2681.
(42) Barrère, F.; van der Valk, C. M.; Dalmeijer, R. A. J.; Meijer, G.; van Blitterswijk, C. A.; de Groot, K.; Layrolle, P. Osteogenecity of Octacalcium Phosphate Coatings Applied on Porous Metal Implants. *J. Biomed. Mater. Res., Part A* **2003**, *66A*, 779−788.
(43) Lim, J. Y.; Shaughnessy, M. C.; Zhou, Z.; Noh, H.; Vogler, E. A.; Donahue, H. J. Surface Energy Effects on Osteoblast Spatial Growth and Mineralization. *Biomaterials* **2008**, *29*, 1776−1784.
(44) Zhao, G.; Raines, A. L.; Wieland, M.; Schwartz, Z.; Boyan, B. D. Requirement for Both Micron- and Submicron Scale Structure for Synergistic Responses of Osteoblasts to Substrate Surface Energy and Topography. *Biomaterials* **2007**, *28*, 2821−2829.
(45) Liu, H.; Cheng, J.; Chen, F.; Hou, F.; Bai, D.; Xi, P.; Zeng, Z. Biomimetic and Cell-Mediated Mineralization of Hydroxyapatite by Carrageenan Functionalized Graphene Oxide. *ACS Appl. Mater. Interfaces* **2014**, *6*, 3132−3140.

DOI: 10.1021/acsami.5b03172
ACS Appl. Mater. Interfaces 2015, 7, 14384−14396